Heavy Double Neutron Stars: Birth, Midlife, and Death

Shanika Galaudage[1,2] , Christian Adamcewicz[1,2] , Xing-Jiang Zhu[1,2] , Simon Stevenson[3,4] , and Eric Thrane[1,2]

[1] School of Physics and Astronomy, Monash University, Clayton VIC 3800, Australia; shanika.galaudage@monash.edu
[2] OzGrav: The ARC Centre of Excellence for Gravitational Wave Discovery, Clayton VIC 3800, Australia
[3] Centre for Astrophysics and Supercomputing, Swinburne University of Technology, Hawthorn, VIC 3122, Australia
[4] OzGrav: The ARC Centre of Excellence for Gravitational Wave Discovery, Hawthorn VIC 3122, Australia
Received 2020 November 3; revised 2021 February 8; accepted 2021 February 19; published 2021 March 11

Abstract

Radio pulsar observations probe the lives of Galactic double neutron star (DNS) systems while gravitational waves enable us to study extragalactic DNS in their final moments. By combining measurements from radio and gravitational-wave astronomy, we seek to gain a more complete understanding of DNS from formation to merger. We analyze the recent gravitational-wave binary neutron star mergers GW170817 and GW190425 in the context of other DNS known from radio astronomy. By employing a model for the birth and evolution of DNS, we measure the mass distribution of DNS at birth, at midlife (in the radio), and at death (in gravitational waves). We consider the hypothesis that the high-mass gravitational-wave event GW190425 is part of a subpopulation formed through unstable case BB mass transfer, which quickly merge in $\sim$10–100 Myr. We find only mild evidence to support this hypothesis and that GW190425 is not a clear outlier from the radio population as previously claimed. If there are fast-merging binaries, we estimate that they constitute 8%–79% of DNS at birth (90% credibility). We estimate the typical delay time between the birth and death of fast-merging binaries to be $\approx$5–401 Myr (90% credibility). We discuss the implications for radio and gravitational-wave astronomy.

Unified Astronomy Thesaurus concepts: Neutron stars (1108); Gravitational waves (678); Binary pulsars (153)

1. Introduction

Radio and gravitational-wave astronomy enable us to study double neutron stars (DNS) at different stages of binary evolution. Radio observations, which probe DNS at midlife, have so far provided precise mass measurements for 12 Galactic DNS (see, e.g., Table 1 in Zhu & Ashton 2020 and references therein). In the standard formation scenario, a DNS consists of two neutron stars: a first-born "recycled" neutron star sped up from accretion and a second-born "slow" neutron star. With relatively few measurements, it is not yet possible to precisely measure the distribution of DNS component masses, but current observations of Galactic DNS are consistent with the following hypotheses: the recycled neutron star mass is distributed according to a double-Gaussian distribution with peaks at $\mu_1 \approx 1.34\,M_\odot$, $\mu_2 \approx 1.47\,M_\odot$, while the slow neutron star mass is distributed uniformly on the interval 1.16–1.42 $M_\odot$ (Farrow et al. 2019).

Based on these fits, one may conclude that most DNS are relatively low mass: 95% of recycled neutron stars have masses less than 1.64 $M_\odot$ while 95% of slow neutron stars have masses less than 1.43 $M_\odot$. Curiously, pulsars in binaries with white dwarfs are regularly found with much larger masses; for example, the mass of PSR J0740+6620 is measured to be $\sim$2.14 $M_\odot$ (Cromartie et al. 2020). Population synthesis studies have explored the DNS populations in the Milky Way, modeling the Galactic population of DNS and understanding the difference between the radio and gravitational-wave populations (Vigna-Gómez et al. 2018; Chattopadhyay et al. 2020; Kruckow 2020; Mandel et al. 2021).

Gravitational-wave astronomy probes only the final moments of DNS. To date, LIGO–Virgo (Aasi et al. 2015; Acernese et al. 2015) have reported the discovery of two DNS mergers: GW170817 (Abbott et al. 2017) and GW190425 (Abbott et al. 2020). While the component masses of GW170817 are consistent with the masses of Galactic DNS,

Abbott et al. (2020) argue it is difficult to explain GW190425, with a primary mass of $1.60\,M_\odot$–$1.87\,M_\odot$ (90% credibility, low-spin prior), as a member of the Galactic radio population. This difficulty has led to speculation about the origin of GW190425.

Romero-Shaw et al. (2020) argue that GW190425 is best understood as a fast-merging binary, which underwent unstable case BB mass transfer. They speculate that GW190425 could have formed from a progenitor including a 4–5$M_\odot$ He star with a $\sim$3$M_\odot$ CO core capable of producing a $\sim$2$M_\odot$ neutron star (Müller et al. 2016; Ertl et al. 2020). According to this hypothesis, massive DNS like GW190425 are not observed in the radio because they merge before they are likely to be seen. This fast-merging hypothesis seems to rely on the premise that the most massive slow-merging DNS are disrupted by large supernova kicks. In the Appendix, we present the results of a population synthesis study to show that large kicks $\gtrsim$2000 km s^{-1} are required for this theory to have explanatory power.

Meanwhile, Safarzadeh et al. (2020) argue that binaries like GW190425 are common in the Milky Way, but we do not see them because the magnetic field of such massive binaries is buried through accretion. Abbott et al. (2020) also float the hypothesis that GW190425 could have been dynamically assembled, but this seems unlikely; numerical simulations suggest neutron star tend to be expelled from the cores of the dense stellar environment, leading to low rates of dynamical mergers (Grindlay et al. 2006; Bae et al. 2014; Belczynski et al. 2018; Papenfort et al. 2018; Zevin et al. 2019; Ye et al. 2020).[5] A range of arguably more exotic hypotheses have been put forward as well, for example, that the primary object in GW190425 could be a black hole (Clesse & Garcia-

---

[5] Andrews & Mandel (2019) posit that there are observational hints of dynamically assembled DNS, despite pessimistic predictions from numerical studies.

Bellido 2020; Foley et al. 2020; Gupta et al. 2020; Kyutoku et al. 2020).

In order to understand how GW190425 formed, it is necessary to introduce a unified framework, which simultaneously accounts for radio and gravitational-wave observations. Selection effects are likely to make the radio-visible and gravitational-wave populations disparate. However, the two populations are linked by the population of DNS at birth. By modeling the population properties of DNS at birth, and then evolving the population through midlife to death, we simultaneously fit data from radio and gravitational-wave astronomy. The remainder of this paper is organized as follows. In Section 2, we introduce a formalism for estimating the birth properties of DNS using measurements from both gravitational waves and radio. In Section 3, we apply our analysis to the two LIGO–Virgo DNS mergers and the 12 radio DNS in order to estimate the population properties of DNS at birth, midlife, and death. Finally, in Section 4, we discuss the implications of our results and future work.

2. Method

We outline a method of inferring the birth mass distributions from observations of radio-visible DNS and binary neutron star mergers. In Section 2.1, we introduce an observationally motivated model (based on Farrow et al. 2019) for the mass distribution of the DNS population at birth. We describe models for the evolution of the DNS formation rate density within the Milky Way (Galactic) and in the greater universe (extragalactic). In Section 2.2, we describe how to evolve the birth mass distribution in time to obtain the radio-visible and gravitational-wave populations. We describe our model for the distribution of delay time between binary formation and merger. In Section 2.3, we describe a formalism to infer the population properties of DNS from data.

2.1. Modeling the DNS Population at Birth

We parameterize the mass distribution of DNS at birth, building on mass models from Farrow et al. (2019). These models explored the radio-visible mass distribution for slow and recycled neutron stars. For simplicity, we assume the recycled and slow neutron star mass distributions are independent. We take the model used for radio-visible DNS as a starting point to describe the DNS mass distribution at birth. Farrow et al. (2019) provide parameterized fits for the distributions of slow and recycled neutron stars in DNS. Their best-fit model for slow neutron stars was a uniform distribution, but we opt to use a Gaussian, which is also consistent with radio data.

Our model for the mass distribution of slow neutron stars $\pi(m_s)$ is a double Gaussian,

$$\pi(m_s|\xi_s, \mu_{si}, \sigma_{si}) = \xi_s \mathcal{N}(\mu_{s1}, \sigma_{s1}) + (1 - \xi_s)\mathcal{N}(\mu_{s2}, \sigma_{s2}), \quad (1)$$

where the distribution $\mathcal{N}(\mu_{s1}, \sigma_{s1})$ is a normalized Gaussian distribution for the low-mass peak with mean μ_{s1} and width σ_{s1}, and $\mathcal{N}(\mu_{s2}, \sigma_{s2})$ is a normalized Gaussian distribution for the high-mass peak with mean μ_{s2} and width σ_{s2}. The subscripts 1 and 2 refer to the low- and high-mass peaks, respectively. We argue below that that the radio population can be understood as coming from peak 1 while the gravitational-wave population includes both peaks 1 and 2.

The high-mass peak is an addition to the model put forward in Farrow et al. (2019). This peak is motivated by GW190425 and the existence of a high-mass peak at ∼1.8 $M_\odot$ in the mass distribution of neutron stars in binaries with white dwarfs (Kiziltan et al. 2013; Alsing et al. 2018). Motivated by the arguments put forth in Romero-Shaw et al. (2020), we posit that this peak is associated with a fast-merging DNS population formed through a stage of unstable case BB mass transfer.[6] In this scenario, the DNS progenitor undergoes a second phase of common-envelope evolution, which involves a neutron star and a helium star with a carbon–oxygen core. At the end of this evolution, the helium envelope gets ejected, resulting in a tight binary (Dewi & Pols 2003; Ivanova et al. 2003). It is hypothesized that high-mass (second-born) neutron stars are preferentially associated with this scenario because the binary is likely to be disrupted (during the second supernova) without being in a sufficiently tight orbit (assuming large supernova kicks for high-mass neutron stars). We note that the recycling process usually refers to stable case BB mass transfer. For the unstable mass transfer that leads to the second common envelope described above, the exact amount of accretion is not well understood; MacLeod & Ramirez-Ruiz (2014) found an estimate of 0.05–0.1 $M_\odot$ but Tauris et al. (2017) adopted an upper limit of 0.01 $M_\odot$.

For the recycled distribution, we use the preferred model from Farrow et al. (2019):

$$\pi(m_r|\xi_r, \mu_{ri}, \sigma_{ri}) = \xi_r \mathcal{N}(\mu_{r1}, \sigma_{r1}) + (1 - \xi_r)\mathcal{N}(\mu_{r2}, \sigma_{r2}), \quad (2)$$

where the distribution $\mathcal{N}(\mu_{r1}, \sigma_{r1})$ is a normalized Gaussian distribution for the low-mass peak with mean μ_{r1} and width σ_{r1}, and $\mathcal{N}(\mu_{r2}, \sigma_{r2})$ is a normalized Gaussian distribution for the high-mass peak with mean μ_{r2} and width σ_{r2}. Note that the high-mass peak in the recycled distribution is not related to the fast-merging channel associated with the high-mass peak in the slow visible DNS population; it is the neutron star population feature of the recycled radio-visible distribution. Example plots of mass distributions of recycled and slow neutron stars are shown in Figure 1. This fiducial population is characterized by parameters provided in Table 1. We return to this fiducial distribution throughout as an illustrative example.

In order to understand how the DNS mass distribution evolves in time, we need to model the DNS birth rate density R_b over cosmic time. We use two models for birth rate density: one for the DNS formation rate in the Milky Way and another for the extragalactic population. For the DNS formation rate in the Milky Way, we model the rate density as constant over cosmic time; see Snaith et al. (2015) Figure 7. We assume the extragalactic DNS formation rate tracks the Madau & Dickinson (2014) model for comoving volumetric star formation rate density as a function of redshift:

$$R_b(t) \propto \psi(z(t)) = 0.015 \frac{(1 + z(t))^{2.7}}{1 + [(1 + z(t))/2.9]^{5.6}}, \quad (3)$$

where $\psi(z)$ is in units of $M_\odot \, \text{yr}^{-1} \, \text{Mpc}^{-3}$. Moving forward, we distinguish between the Galactic and extragalactic DNS populations, carrying out parallel calculations (outlined in

---

[6] While the stable case BB mass transfer process was capable of explaining observations prior to GW190425, the unstable mass transfer hypothesis was invoked to reconcile GW190425 and radio DNS observations.
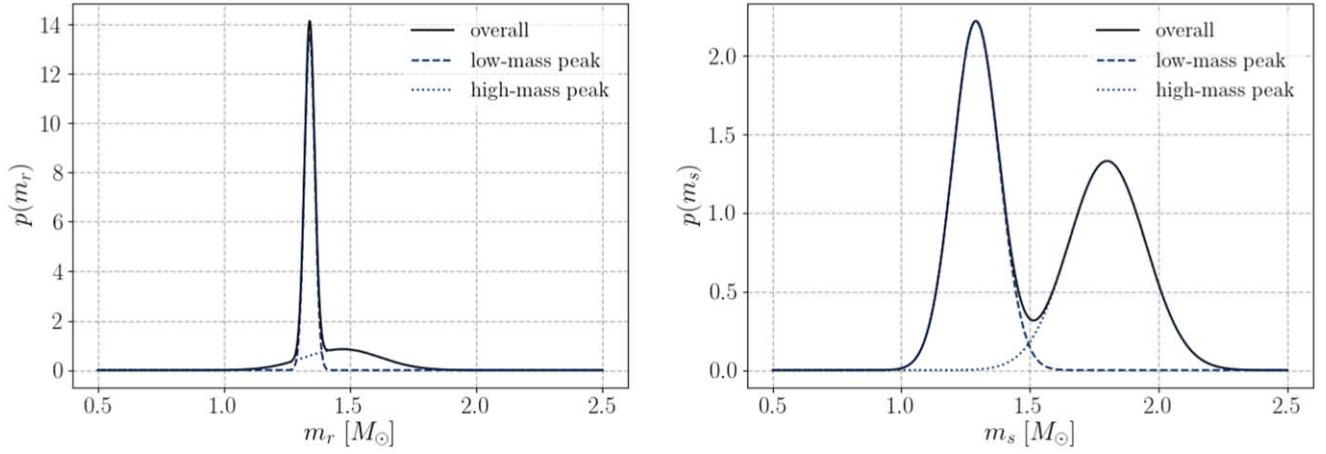
Figure 1. Example birth mass distributions for recycled (left) and slow (right) neutron stars assuming the fiducial population parameters given in Table 1. The dashed line traces the low-mass peak, the dotted line traces the high-mass peak, and the solid line is the overall distribution. The high-mass peak in the distribution of slow neutron stars corresponds to fast-merging binaries, which we posit are not frequently seen in radio due to selection effects.

Table 1
Fiducial Population Parameters Describing an Example Population of Double Neutron Stars at Birth

Parameter	Description	Recycled	Slow
ξ	Fraction of binaries in the low-mass peak	0.68	0.5
μ_1	Mean of low-mass peak	1.34 $M_\odot$	1.29 $M_\odot$
σ_1	Width of low-mass peak	0.02 $M_\odot$	0.09 $M_\odot$
μ_2	Mean of high-mass peak	1.47 $M_\odot$	1.8 $M_\odot$
σ_2	Width of high-mass peak	0.15 $M_\odot$	0.15 $M_\odot$

Note. See Equations (1)–(2) for parameter definitions. The population is plotted in Figure 1.

Section 2.2) for each population, but assuming different birth rate densities.

2.2. Evolving the DNS Population: Midlife and Death

Using the birth mass distribution and the birth rate density, we can evolve the population in time. The DNS merger rate density (which is a snapshot of the gravitational-wave population) is given by the convolution of the birth rate density with the delay-time distribution:

$$R_m(t) = \int_0^t dt_b \, R_b(t_b)\pi(t - t_b). \quad (4)$$

Here, $R_m(t)$ is the merger rate density as a function of cosmic time while $R_b(t)$ is the DNS formation rate density. We measure time t relative to the beginning of the binary formation $\approx$13 Gyr ago, which coincides roughly with the origin of the Galaxy at $t = 0$. The variable t_b is the birth time of the binary and $\pi(t - t_b)$ is the probability density function for the delay time between birth and merger.

We employ two models for the time delay distribution: one for conventional (slow) mergers and one for fast mergers. The conventional model assumes a distribution that is uniform in the logarithm of time delay with a minimum delay time of 30 Myr:

$$\pi(t_d) \propto \begin{cases} 0 & t_d \leqslant 30 \text{ Myr} \\ 1/t_d & t_d > 30 \text{ Myr} \end{cases}; \quad (5)$$

see, for example, Figure 3 in Neijssel et al. (2019). The second model is motivated by our desire to accommodate potentially fast-merging binaries such as GW190425. We use a delta-function distribution for the delay-time distribution of the fast-merging channel,

$$\pi(t_d) = \delta(t_d - t_*). \quad (6)$$

This choice is motivated by the necessity to enforce that this secondary channel is, in fact, fast merging. A wide time delay distribution does not place such a constraint on the secondary channel, as DNS under these circumstances are still free to merge on a similar timescale to the standard channel. Preliminary testing found that a Gaussian distribution of time delay produced results nearly identical to that of a delta-function distribution. As such, we opt for the former to simplify our model. As in Romero-Shaw et al. (2020), we assume a fiducial fast-merger time of $t_* = 10$ Myr (Abbott et al. 2020; Romero-Shaw et al. 2020). However, we also present results where t_* is treated as a free parameter, allowed to take on values from 5 to 500 Myr. Using our prescription for formation rate density and delay-time distribution, we can obtain the merger rate density distribution. The left panel of Figure 2 shows the DNS formation rate density and the merger rate densities for the slow- (Equation (5)) and fast- merging (Equation (6)) channels; in these plots, we assume $t_* = 10$ Myr. These rate densities are in arbitrary units.

Now let us consider the radio-visible DNS population. Using the DNS formation and merging rate densities, we can calculate the number of radio-bright binaries in the Galaxy given by

$$N_r(t) = \int_0^t dt'(R_b(t') - R_m(t'))\epsilon(t'). \quad (7)$$

Here, ϵ describes the fraction of midlife DNS in the Galaxy which are radio-visible. If we temporarily ignore the ϵ factor for a moment (setting it to one), the number of radio-bright binaries is simply given by the number that have been born over the interval $(0, t)$ minus the number that have merged, and so are no longer visible. However, not every yet-to-merge binary is visible in radio. Something like 10% of neutron stars are visible because they are not beamed toward
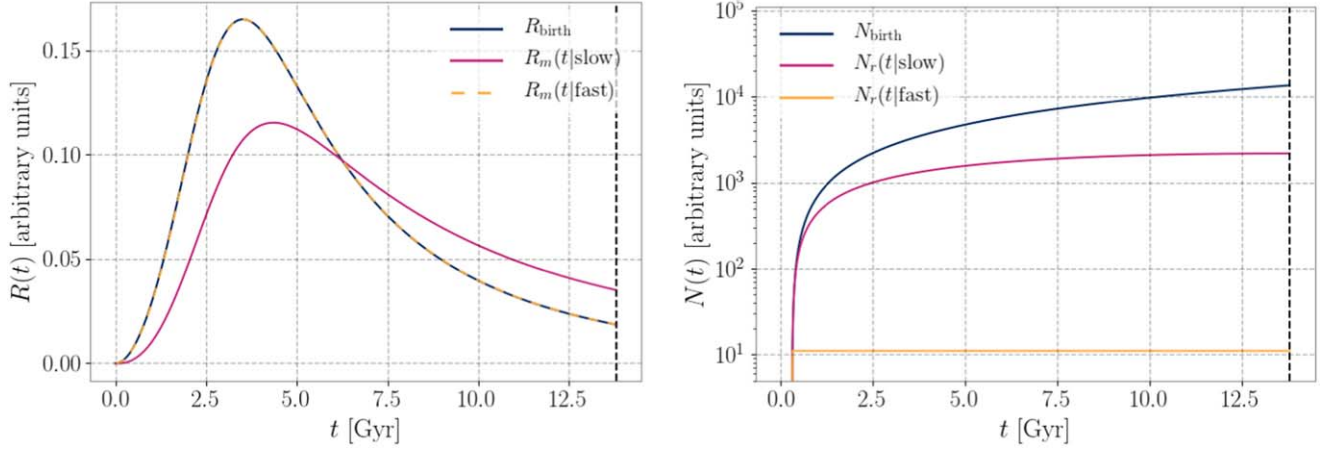
3

Figure 2. Comparison of the merger rate densities and number of radio-visible binaries in the slow-merging channel and the fast-merging channel. Left: merger rate density (arbitrary units) for different delay-time channels for an extragalactic population assuming the Madau–Dickinson model for the DNS formation rate density. Right: number of binaries visible in radio (arbitrary units) for different delay-time channels for the Milky Way population assuming a uniform distribution for the DNS formation rate density. The black dashed lines represent t_{today}.
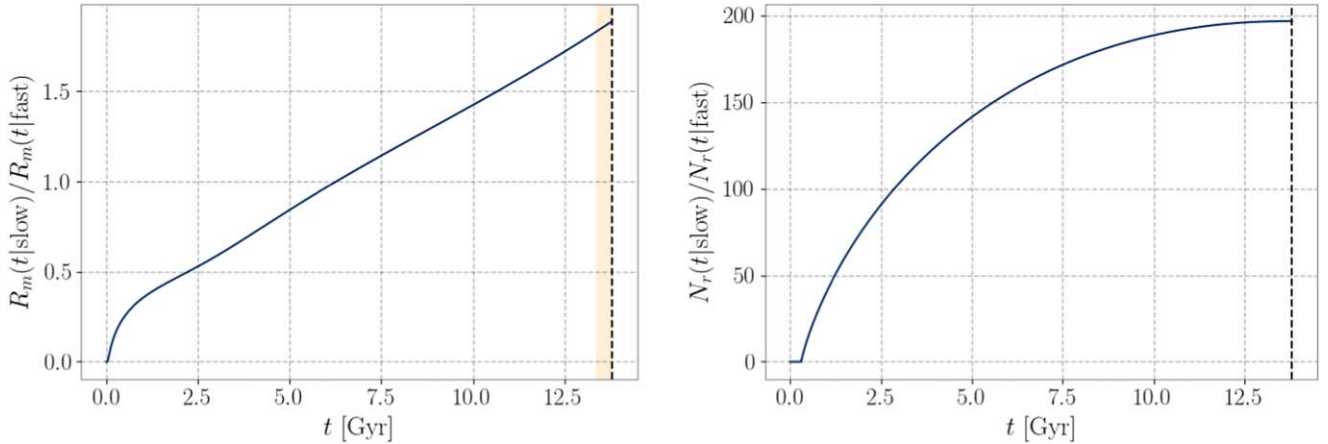

Figure 3. The ratio of the merger rate and number of radio-visible binaries in the slow-merging channel and the fast-merging channel. Left: merger rate ratio of the binaries in different delay-time channels for extragalactic population assuming the Madau–Dickinson model for the DNS formation rate density. The shaded region (yellow) represents the detection horizon for gravitational-wave mergers. Right: ratio of the number of binaries visible in radio for different delay-time channels for the Milky Way population assuming a uniform distribution for the DNS formation rate density. The black dashed lines represent t_{today}.

Earth (O'Shaughnessy & Kim 2010; Thrane et al. 2020), and so we expect $\epsilon(t) \approx 0.10$. Moreover, it is possible that ϵ is time dependent if we expect pulsars to grow dim as they age (Bransgrove et al. 2018; Zhu et al. 2018). For the sake of simplicity, we ignore this possibility for the time being, though this time dependence is worth exploring in future work.

The right-side panel of Figure 2 shows the number of DNS at birth (navy), the number of radio-visible DNS in the slow channel (magenta), and the number of radio-visible DNS in the fast-merging channel (yellow). The distribution of fast-merging binaries has a lower number of radio binaries compared to the slow-merging binaries. In practice, there are significant uncertainties associated with $R_b(t)$ and $\epsilon(t)$. However, if we consider two different models, slow merging and fast merging for the delay-time distribution, and if we know the ratio of the current merger rate densities for these two channels,

$$\frac{R_m(t|\mathrm{slow})}{R_m(t|\mathrm{fast})}, \tag{8}$$

then we can precisely predict the ratio of currently visible radio binaries for these two models,

$$\frac{N_r(t|\mathrm{slow})}{N_r(t|\mathrm{fast})}. \tag{9}$$

The overall normalizations of R_b and ϵ drop out of the ratio.

Figure 3 shows the slow-to-fast ratio of merger rate densities (left) and the slow-to-fast ratio of radio-visible binaries (right). The ratio of fast-merging DNS to slow-merging DNS today is 1.88. However, the radio-visible DNS in the fast-merging channel is highly suppressed; the ratio of slow merging to fast merging is 196. This illustrates how GW190425 could have been part of a fast-merging population (with a merger rate comparable to slow-merging DNS) while accounting for the lack of comparably massive radio-visible DNS. We calculate these ratios assuming that LIGO–Virgo (and radio observations) are sensitive to DNS in the local universe: $z \approx 0$. However, we note that as gravitational-wave detectors become more sensitive, it will be possible to probe DNS mergers over sufficiently large spans of cosmic time. Thus, it will eventually
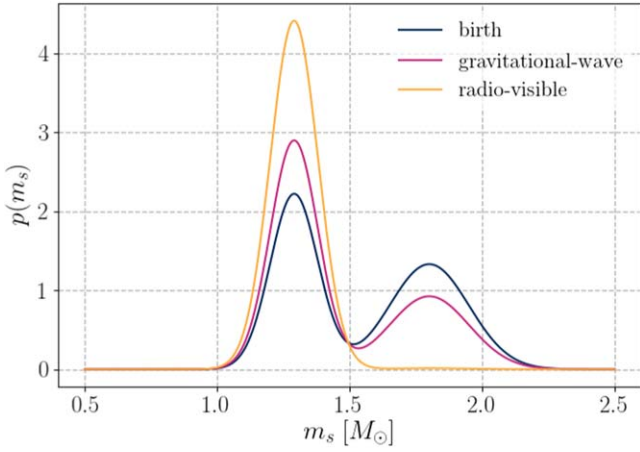
Figure 4. The mass distribution of slow neutron stars at birth (blue), merging (magenta), and in radio (yellow). The high-mass peak is suppressed in radio by a factor of $\zeta_{\mathrm{radio}} = 196$. Here, we have assumed that fast-merging binaries merge in $t_* = 10$ Myr.

become necessary to take into account the evolving merger rate.

The slow-to-fast-merger rate density ratio ($\zeta_{\mathrm{GW}} = 1.88$) and the slow-to-fast ratio of radio binaries ($\zeta_{\mathrm{radio}} = 196$) serve as transfer functions that describe how the relative mixture of slow-to-fast evolves from birth to radio binaries to gravitational-wave mergers. The radio and gravitational-wave distributions of slow neutron stars are given by

$$\pi_x(m_s | \xi_s, \mu_{si}, \sigma_{si})$$
$$= \eta_x \zeta_x \xi_s \mathcal{N}(\mu_{s1}, \sigma_{s1}) + \eta_x (1 - \xi_s) \mathcal{N}(\mu_{s2}, \sigma_{s2}), \quad (10)$$

where $x = $ GW employs the gravitational-wave transfer function and $x = $ radio employs the radio transfer function. Meanwhile, η is a normalization factor:

$$\eta_x = \frac{1}{(\zeta_x - 1)\xi_s + 1}, \quad (11)$$

where ζ_{GW} is the transfer function weight from the merger number ratio and ζ_{radio} is the transfer function weight from the radio number ratio; recall that ξ_s is the fraction of slow-merging binaries produced at birth (Equation (1)). Figure 4 shows the birth DNS distribution for slow mass and the resulting radio and gravitational-wave distributions.

2.3. Inferring the Birth Parameters

Having related the radio and gravitational-wave populations to the birth distribution, we can combine the radio and gravitational-wave data to infer the birth mass distribution. The likelihood of the data given population parameters Λ is the product of the gravitational-wave and radio likelihoods:

$$\mathcal{L}(d | \Lambda) = \prod_i^M \mathcal{L}_{\mathrm{GW}}(d_i | \Lambda) \prod_j^N \mathcal{L}_{\mathrm{radio}}(d_j | \Lambda). \quad (12)$$

The population parameters Λ describe the shape of the DNS mass distribution at birth. The prior distributions of these parameters are summarized in Table 2. We assume a uniform prior $U(0, 1)$ for ξ_s, the fraction of slow neutron stars in the low-mass Gaussian. Some population studies (e.g., Safarzadeh et al. 2020) suggest that the fraction of fast-merging binaries is

relatively small $\lesssim 10\%$, which would correspond to a prior peaked at $\xi_s \approx 90\%$. However, we take a data-driven approach so that all values of ξ_s are given equal prior weight.

Taking into account selection effects (Thrane & Talbot 2019; Vitale et al. 2020), the likelihood is

$$\mathcal{L}(d | \Lambda, \, \mathrm{det}) = \left(\frac{1}{p_{\mathrm{det, GW}}(\Lambda)} \right)^M \prod_i^M \mathcal{L}_{\mathrm{GW}}(d_i | \Lambda)$$
$$\times \left(\frac{1}{p_{\mathrm{det, radio}}(\Lambda)} \right)^N \prod_j^N \mathcal{L}_{\mathrm{radio}}(d_j | \Lambda). \quad (13)$$

Here, p_{det} is the probability of detecting the DNS. For gravitational events,

$$p_{\mathrm{det, \, GW}} \approx \mathcal{M}^{5/2}, \quad (14)$$

where $\mathcal{M}$ is the chirp mass,

$$\mathcal{M} = \frac{(m_1 m_2)^{3/5}}{(m_1 + m_2)^{1/5}}, \quad (15)$$

and m_1 and m_2 are the primary and secondary masses of the compact binary, respectively. The recycled and slow masses are related to the primary and secondary masses as follows,

$$m_1 = \max(m_r, m_s) \quad (16)$$
$$m_2 = \min(m_r, m_s). \quad (17)$$

There are two types of selection effects one can imagine at play with the radio population. Fast-merging binaries are not visible in radio. Therefore, the population we see in the radio is not representative of the birth population. However, we already take this into account with the transfer function ζ_{radio}. Here, we are concerned with how the radio population detectability varies with mass. We assume that this variation is negligible and so we set $p_{\mathrm{det, \, radio}} = 1$.

We rewrite the likelihood as a sum that recycles posterior samples; see, e.g., (Thrane & Talbot 2019),

$$\mathcal{L}(d | \Lambda, \, \mathrm{det})$$
$$= \left(\frac{1}{p_{\mathrm{det, GW}}(\Lambda)} \right)^M \prod_i^M \frac{\mathcal{L}_{\mathrm{GW}}(d_i | \Lambda_0)}{n_i} \sum_k^{n_i} \frac{\pi(\theta_{i,k} | \Lambda)}{\pi(\theta_{i,k} | \Lambda_0)}$$
$$\times \left(\frac{1}{p_{\mathrm{det, radio}}(\Lambda)} \right)^N \prod_j^N \frac{\mathcal{L}_{\mathrm{radio}}(d_j | \Lambda_0)}{n_j} \sum_k^{n_j} \frac{\pi(\theta_{j,k} | \Lambda)}{\pi(\theta_{j,k} | \Lambda_0)}. \quad (18)$$

where Λ_0 is the fiducial population parameter values used for the initial analysis of individual DNS. We evaluate Equation (18) using GWPOPULATION, a population inference package for gravitational-wave analyses based on BILBY Ashton et al. (2019). We use the nested sampler DYNESTY (Speagle 2020). The recycled and slow-mass posteriors for the gravitational-wave events are from analyses by Zhu & Ashton (2020) and the posteriors for the radio observations are from Farrow et al. (2019).

3. Results

We analyze the 12 radio-visible DNS (Jacoby et al. 2006; Kramer et al. 2006; Weisberg et al. 2010; Lynch et al. 2012, 2018; Ferdman et al. 2014, 2020; Fonseca et al. 2014; Martinez et al. 2015; van Leeuwen et al. 2015; Cameron et al.

Table 2
Prior Distributions for the Hyperparameters

Parameter	Description	Prior
ξ_r	Fraction of recycled neutron stars in low-mass Gaussian	$U(0, 1)$
μ_{r1}	Mean of low-mass Gaussian in m_r distribution	$U(1.1M_\odot, 1.5M_\odot)$
σ_{r1}	Standard deviation of low-mass Gaussian in m_r distribution	$U(0.005M_\odot, 0.5M_\odot)$
μ_{r2}	Mean of high-mass Gaussian in m_r distribution	$U(\mu_{r1}, 2.0M_\odot)$
σ_{r2}	Standard deviation of high-mass Gaussian in m_r distribution	$U(0.005M_\odot, 0.5M_\odot)$
ξ_s	Fraction of slow neutron stars in low-mass Gaussian	$U(0, 1)$
μ_{s1}	Mean of low-mass Gaussian in the m_s distribution	$U(1.1M_\odot, 1.5M_\odot)$
σ_{s1}	Standard deviation of a low-mass Gaussian in the m_s distribution	$U(0.005M_\odot, 0.5M_\odot)$
μ_{s2}	Mean of high-mass Gaussian in the m_s distribution	$U(\mu_{s1}, 2.0M_\odot)$
σ_{s2}	Standard deviation of high-mass Gaussian in the m_s distribution	$U(0.005M_\odot, 0.5M_\odot)$
$m_{\min}$	Minimum possible neutron star mass	$1M_\odot$
$m_{\max}$	Maximum possible neutron star mass	$3M_\odot$
t_*	Characteristic delay time	$U(5\ \mathrm{Myr}, 500\ \mathrm{Myr})$

Note. The notation $U(a, b)$ indicates a uniform distribution on the interval ranging from a to b.

2018; Haniewicz et al. 2021) and 2 binary neutron star mergers from LIGO–Virgo (Abbott et al. 2017, 2020). In Figure 5, we plot the reconstructed recycled and slow neutron star mass spectra. The top panel shows the mass distribution of recycled neutron stars, and the bottom panel shows the mass distribution of slow neutron stars. The solid curves are the population predictive distributions (the best-guess reconstruction, averaged over population parameters), and the shaded regions represent the 90% credible regions. The birth population is shown in navy. The merging population observed in gravitational waves is shown in magenta. The radio-visible population is shown in yellow. In the mass distribution of recycled neutron stars, the birth, merging, and radio distributions are identical. In the mass distribution of slow neutron stars, the birth, merging and radio distributions differ substantially. Fast-merging, high-mass binaries present in the birth distribution are suppressed in the radio distribution (by a factor of $\zeta_{\mathrm{radio}} \approx 4$–74 at 90% credibility) because they do not live long enough to be observed. Fast-merging binaries are suppressed in the merging population by a modest factor of $\zeta_{\mathrm{GW}} \approx 1.8$ (see Figure 9 for distributions of the transfer function weights).

In Figures 6–7, we provide posterior corner plots for the recycled and slow population parameters. The shaded regions indicate the 1σ, 2σ, and 3σ credible intervals. The high-mass peak in the mass distribution of slow neutron stars associated with the fast-merging channel visible in Figure 5 is also shown in Figure 7, which shows mild support for a broad peak at $\mu_{s2} \approx 1.62M_\odot$. We rule out the hypothesis that all DNS are from the high-mass peak at high credibility. There is only mild support for the existence of a high-mass peak (Bayes factor $\mathcal{B} = 2$). While the presence of a fast-merging channel is slightly preferred, $\xi_s < 1$, the data are consistent with the hypothesis that no binaries merge swiftly $\xi_s = 1$.

In Figure 8, we plot the mass posteriors for the DNS used in our study. The shaded regions indicate the 1σ level of the low- (yellow) and high-mass (magenta) peaks from our population analyses. The fast-merging channel is represented by the high-

mass peak in the mass distribution of slow neutron stars ($\mu_{s2} = 1.62^{+0.31}_{-0.27}$ at 90% credibility). The heavy DNS merger, GW190425, is associated with this high-mass, fast-merging channel. In Figure 9, we plot the posteriors for the characteristic delay-time distribution and the corresponding distribution for the transfer functions: ζ_{GW}, ζ_{radio}. The shaded regions indicate the 1σ, 2σ, and 3σ credible intervals. We place only weak constraints on the delay-time parameter: $t_* \approx 5$–401 (90% credibility). Each value of t_* corresponds to single values of ζ_{GW} and ζ_{radio}. We find that $\zeta_{\mathrm{GW}} \approx 1.8$ regardless of the value of t_* and that ζ_{radio} ranges from ≈ 4–74 at 90% credibility.

4. Discussion

DNS systems evolve over time: they are born, they live for a period during which they may be seen in radio, and then they merge emitting gravitational waves. It is necessary to model this evolution in order to achieve a clear understanding of DNS systems. We present a model for the DNS birth mass distribution, along with a prescription for DNS evolution, which allows us to combine radio and gravitational-wave observations. Using this framework, we are able to self-consistently measure the population properties of DNS at birth, at midlife (in radio), and at death (in gravitational waves). It also enables us to eschew the conventional primary/secondary distinction of gravitational-wave astronomy in favor of an arguably more physically motivated description involving slow and recycled neutron stars as in Zhu & Ashton (2020).[7]

Hypothesizing that the most massive DNS merge quickly (in ∼ 10–100 Myr) through unstable case BB mass transfer, we find mild evidence for a broad peak at ∼1.6 $M_\odot$ in the birth mass distributions of slow neutron stars (see Figure 7). We find mild support for the hypothesis that the unusually massive

---

[7] See also Biscoveanu et al. (2020), who model compact objects A and B depending on which one is more rapidly spinning.
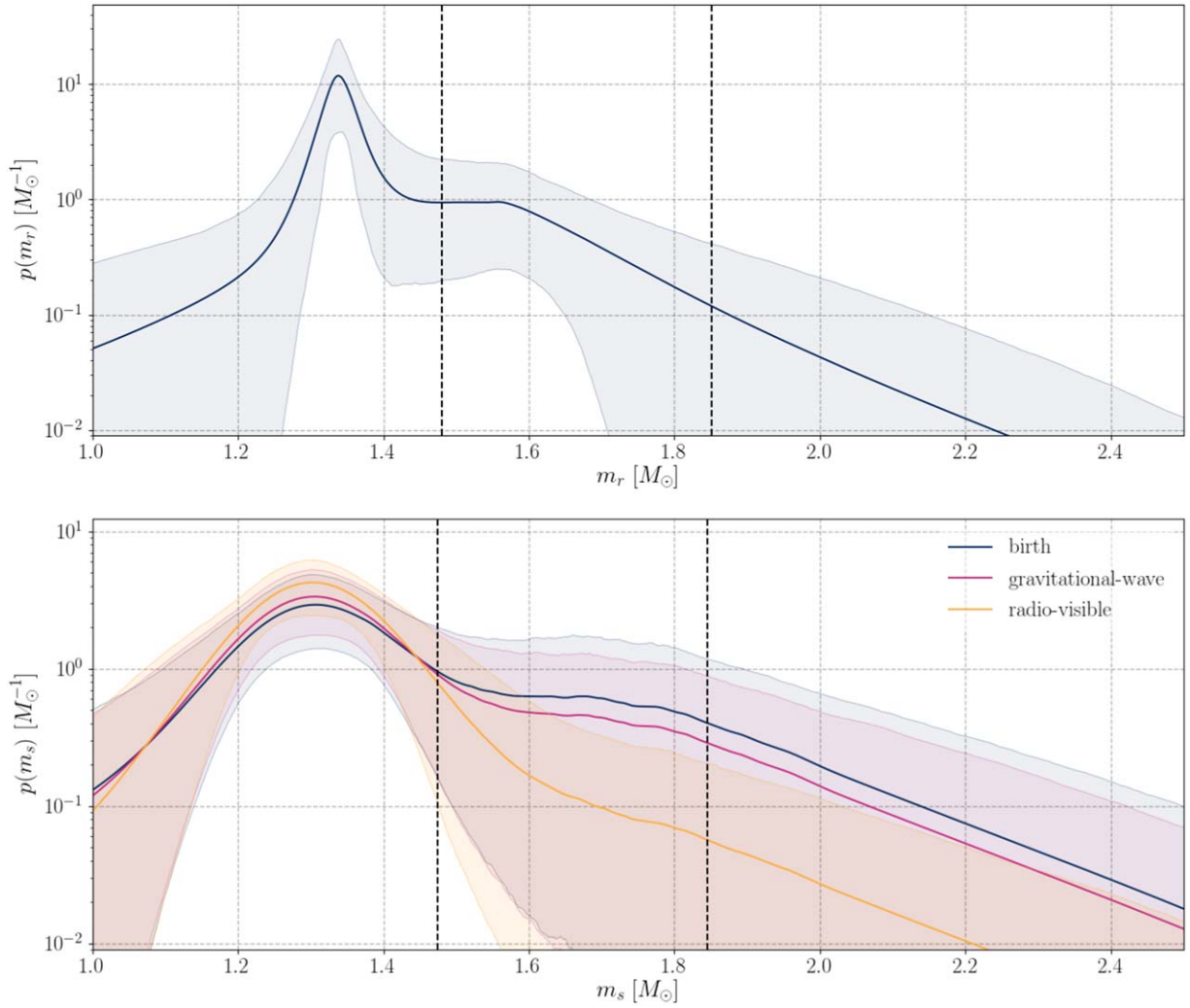
Figure 5. Reconstructed distributions for recycled mass (m_r; above) and slow mass (m_s; below) for the birth (navy), merging (magenta) and radio-visible (yellow) distributions. The solid curves indicate the population predictive distributions, and the shaded regions represent the 90% credible interval. The black dashed lines represent the 90% credible interval of the posterior distribution for GW190425.

DNS system GW190425 can be understood as such a fast-merging system ($\mathcal{B} = 2$), which is consistent with the constraint on the merger time based on the spin measurement reported in Zhu & Ashton (2020). If we fix the delay time of the fast-merging channel to $t_* = 10\,\mathrm{Myr}$, we find slightly more support for this fast-merging scenario ($\mathcal{B} = 4$). We find that $\approx 8\%$–79% of binaries at birth are fast merging. If subsequent detections reveal a stronger discrepancy between the radio and gravitational-wave populations, our model provides a natural explanation for why such massive DNS are not commonly observed in radio because we infer that fast-merging DNS are suppressed in the radio population by a factor of ≈ 4–74 (90% credibility). Our model makes potentially falsifiable predictions about the maximum delay time for fast-merging DNS $t_* \approx 5$–$401\,\mathrm{Myr}$ (90% credibility) and for the prevalence of fast-merging DNS in the Milky Way.

While our study shows that the presence of a fast-merging channel for massive DNS can account for a discrepancy between the Galactic population and the unusually large mass of GW190425, we do not rule out other explanations for the lack of heavy DNS visible in radio. For example, Safarzadeh et al. (2020) argue that massive DNS are relatively common in the Milky Way, but we do not see them in radio because the

magnetic field is buried through accretion. Safarzadeh et al. (2020) argue that the fast-merging hypothesis explored here is in tension with at least some population synthesis studies, which predict a relatively small fraction of fast-merging systems: $\lesssim 10\%$. This estimate is consistent with the low end of our 90% credible interval: 8%–79%. However, theoretical predictions may vary with different population synthesis prescriptions.

It seems challenging to determine which of these two scenarios is more likely to be true observationally because the buried-field hypothesis produces similar predictions to the fast-merging hypothesis. The LISA observatory (Armano et al. 2016) may be able to provide evidence in favor of one hypothesis over the other; if high-mass DNS are plentiful in the Milky way, they should be visible in millihertz gravitational waves, even if they are radio quiet (Andrews et al. 2020; Korol & Safarzadeh 2021; Lau et al. 2020). Alternatively, if radio observatories are able to detect an ultrarelativistic DNS with a merger time of $\lesssim 10\,\mathrm{Myr}$ (Pol et al. 2020) and the system includes an unusually massive neutron star, this would provide
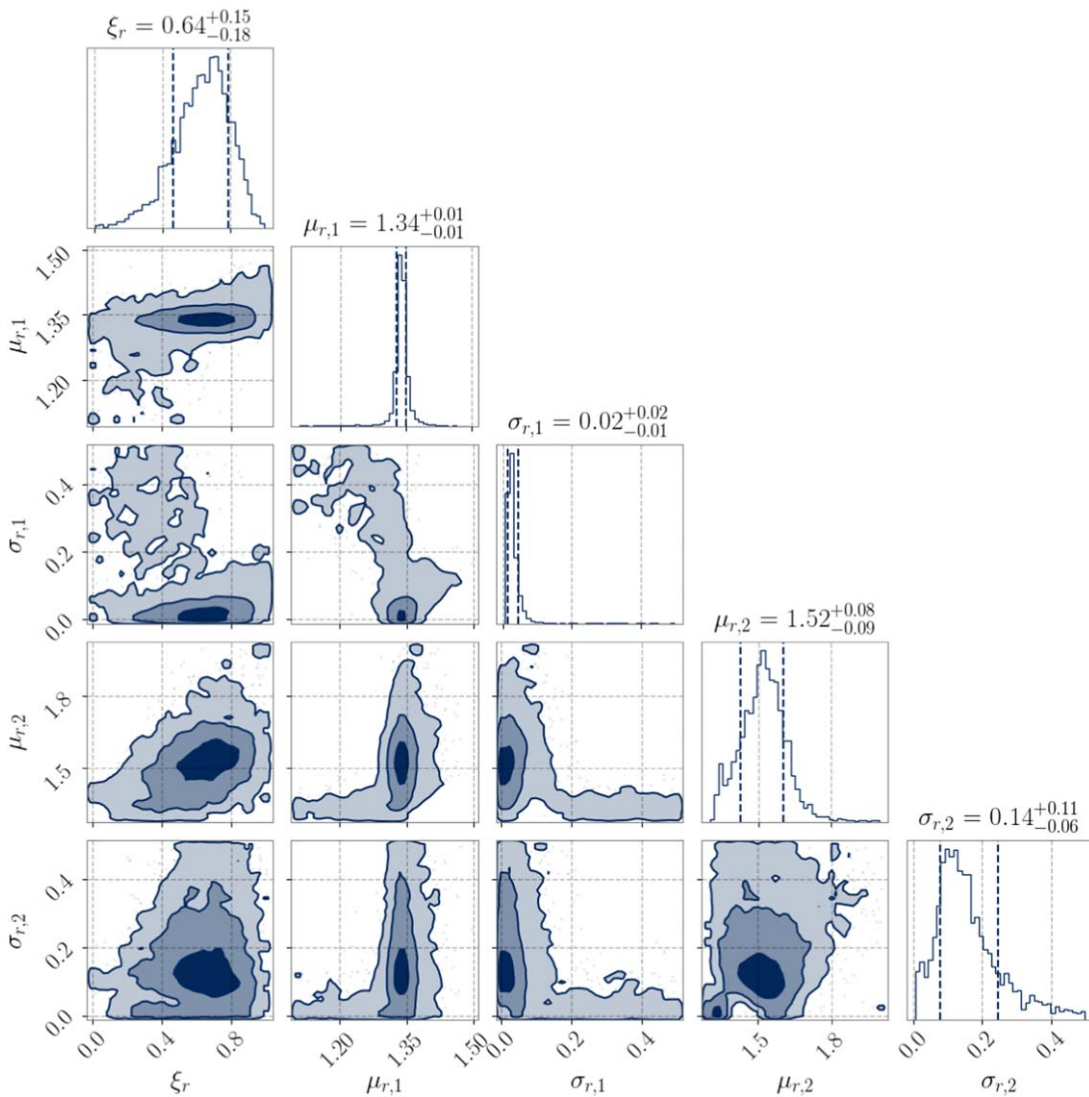
Figure 6. Posterior distributions for the recycled mass population parameters. The credible intervals on the 2D posterior distributions are at 1σ, 2σ and 3σ, using increasingly light shading. The intervals on the 1D posterior distributions are at 1σ.

support for the fast-merging hypothesis.[8] Finally, if radio observatories detect a high-mass DNS system with a long time to merge, such an observation could provide evidence against both the fast-merging hypothesis and the buried-field hypothesis because one would expect such systems to be rare given either hypothesis.

While the analysis here is likely good enough to apply to the current small data set of DNS, there are a number of improvements that will be useful to explore in the future as additional DNS are detected. First, our model uses a simplistic delta-function delay-time distribution for the fast-merging channel. With more DNS, the analysis will become more sensitive to the shape of the delay-time distribution, and it may become necessary to explore more realistic delay-time models. Second, we ignore the possibility that the magnetic field might decay with time (Bransgrove et al. 2018). A more sophisticated treatment could model this field decay. Third, we assume that

all DNS systems are equally detectable in the radio. While this is probably a good approximation for our present purposes, it might be interesting to modify the analysis here to take into account the difficulty detecting ultrarelativistic DNS with radio (Pol et al. 2020). Finally, because all currently known DNS are relatively nearby, we carry out calculations using a zero-redshift approximation. As LIGO–Virgo detect DNS mergers at ever greater distances, it will become possible to observe the changing proportions of slow and fast mergers over cosmic time. Fortunately, we can straightforwardly accommodate this effect by making the radio and gravitational-wave transfer functions redshift-dependent.

Our results suggest that a reasonably large fraction ($\sim$40%) of DNS may merge quickly. If so, the short merger timescales of these systems have a number of implications. Detections of short gamma-ray bursts are typically offset from their host galaxies and in regions where there is little star formation or in globular clusters (Grindlay et al. 2006; Fong & Berger 2013). Although these are fast-merging systems, these tight binaries ($P_{\rm orb} < 1$ hr) can have high kick velocities, which can result in the binary escaping the host galaxy (Andrews & Zezas 2019). If some DNS are found to merge quickly, future work should

---

[8] If the buried-field approach turns out to be right, the framework presented in this paper can be straightforwardly adapted to describe that model instead. For example, the fast-merging, high-mass peak would be reinterpreted as the buried-field, high-mass peak.
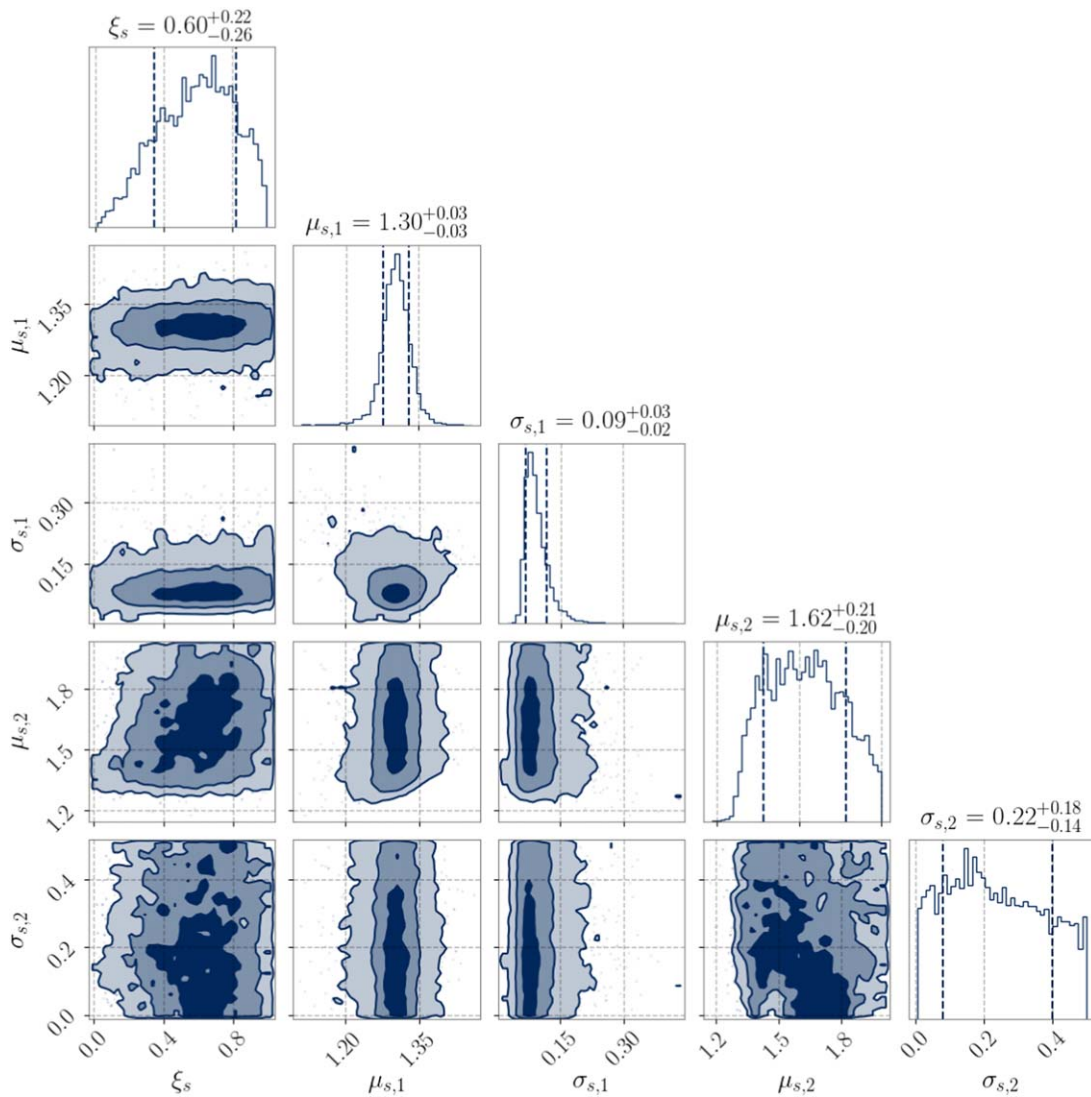
Figure 7. Posterior distributions for the slow-mass population parameters. The credible intervals on the 2D posterior distributions are at 1σ, 2σ and 3σ, using increasingly light shading. The intervals on 1D posterior distributions are at 1σ level.

check for consistency with short gamma-ray burst offsets. Short merging timescales may also help explain r-process enrichment in globular clusters and ultrafaint dwarf galaxies (Ji et al. 2016; Safarzadeh et al. 2019; Kobayashi et al. 2020). However, it is not clear whether they will provide a significant source of enrichment given that the ejected mass from neutron star binaries decreases as the binary mass increases (Radice et al. 2018). We are hopeful that this work will be useful when characterizing the neutron star–black hole mass gap. By combining the DNS mass models here with models for the binary black hole mass spectrum, e.g., Talbot & Thrane (2018) and Abbott et al. (2019), it should be possible to characterize the nature of this gap; see, e.g., Fishbach et al. (2020). Precise measurement of the mass gap may shed light on the minimum and maximum neutron star mass (Chatziioannou & Farr 2020) —or, at least, the minimum and maximum mass of neutron stars in DNS. The maximum neutron star mass has implications for the neutron star equation of state (EoS), which is determined by nuclear physics at the highest possible densities (Breu & Rezzolla 2016; Essick & Landry 2020; Landry et al. 2020).

Appendix

In this Appendix, we investigate the distribution of supernova kicks required for the fast-merging hypothesis of GW190425 to have explanatory power. We carry out a rudimentary population synthesis analysis in order to estimate the typical supernova kick velocities required in order to disrupt a nonnegligible fraction of slow-merging binaries (thereby changing the radio-visible mass distribution) without disrupting the fast-merging binaries created by unstable case BB mass transfer. While some population synthesis analyses assume maximum supernova kicks of $\sim$1000 km s^{-1}, we find
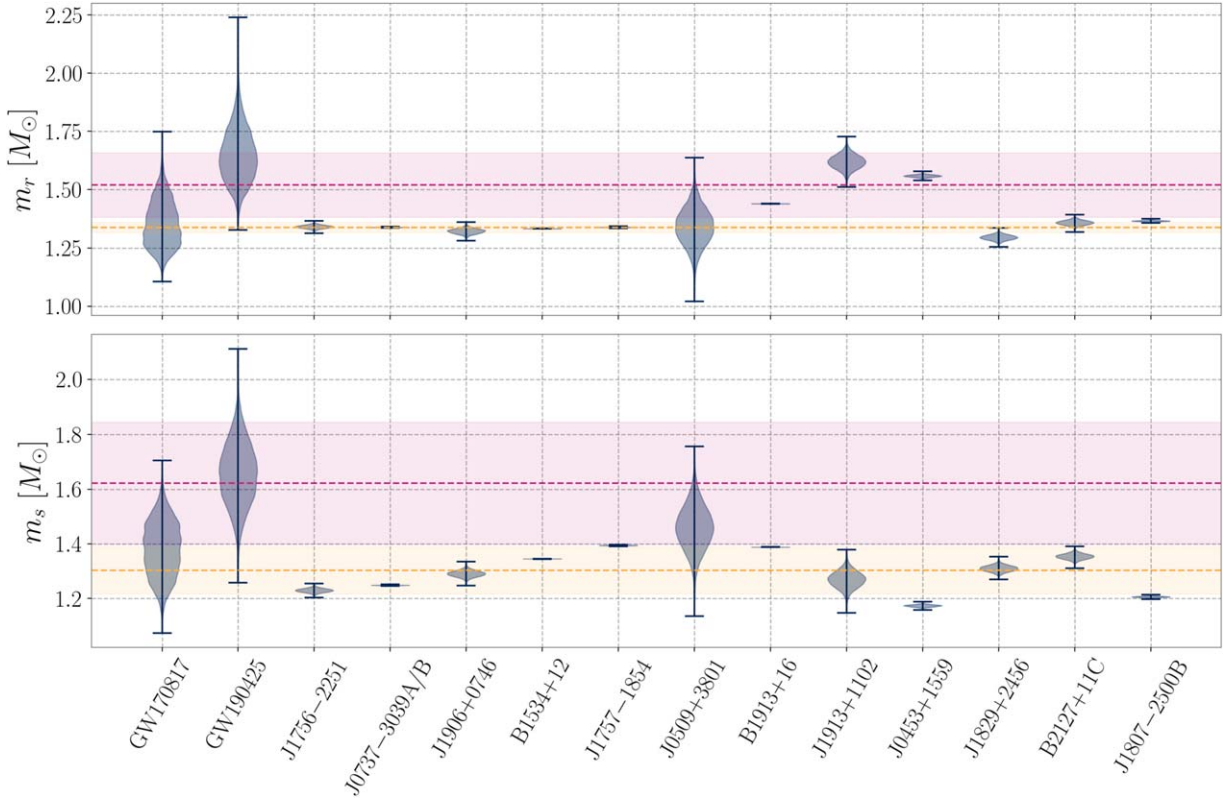
Figure 8. Posterior distributions of recycled and slow mass for the radio and gravitational-wave events. The shaded regions represent the 1σ level of the low- (yellow) and high-mass (magenta) peaks in our mass distributions. Note that, for two globular-cluster pulsars (B2127+11C and J1807−2500B; both recycled), their undetected companions could be either young/slow or recycled neutron stars. The recycled and slow posteriors for the gravitational-wave events are from Zhu & Ashton (2020).
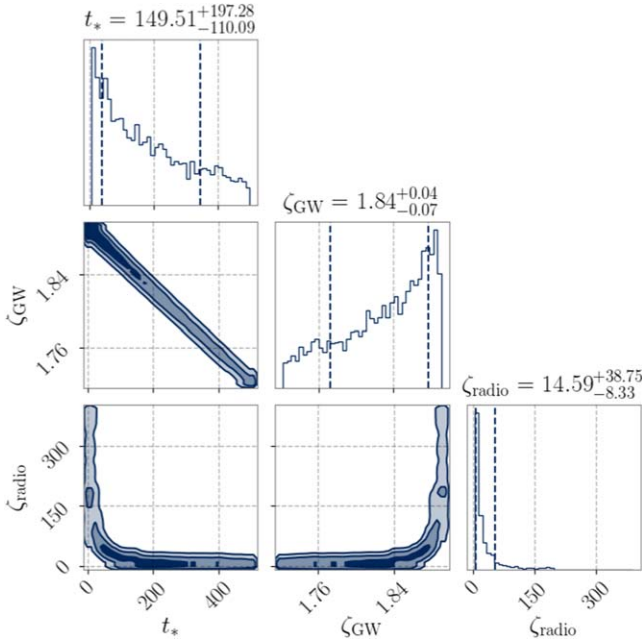

Figure 9. Posterior distributions for the characteristic delay time and transfer function weights. The credible intervals on the 2D posterior distributions are at 1σ, 2σ and 3σ, using increasingly light shading. The intervals on the 1D posterior distributions are at 1σ.

that kicks of $\gtrsim 2000\ \mathrm{km\ s^{-1}}$ are required for the fast-merging hypothesis to have explanatory power. While such large kicks are potentially surprising, the existence of large kicks in at least some cases is supported by observations of high-velocity

pulsars (Chatterjee et al. 2005; Hobbs et al. 2005; Tomsick et al. 2012); we return to the topic of these high-velocity pulsars below.

The first step in our analysis is to assume a relationship between the progenitor carbon–oxygen (CO) core mass m_{core} and the remnant mass m. Different prescriptions assume different relationships. The general trend is for the m_{core} to increase with m (Fryer et al. 2012; Spera et al. 2015), though, this increase may be interrupted by discontinuities (Mandel & Müller 2020). Here, we assume a linear relationship between the core mass and the mass of the slow neutron star:

$$m_{\mathrm{core}} = 2.65 m_s - 0.95. \qquad (\mathrm{A1})$$

As a rule of thumb, larger supernova kick velocities v_{kick} are thought to be associated with larger core masses, although it is possible there is significant stochasticity so that different kicks are possible for a single core mass. We assume a linear relation

$$v_{\mathrm{kick}} = k m_{\mathrm{core}}. \qquad (\mathrm{A2})$$

We treat k as a free parameter and vary it between 100–$800\ \mathrm{km\ s^{-1}}\ M_\odot^{-1}$ in order to find a value that produces sufficiently large kicks to disrupt slow-merging massive binaries. We simulate DNS systems, drawing masses from our mass distributions (Figure 5) and orbital periods from a log-uniform distribution. For the slow-merging channel, the orbital period P_b range is 1–12 hr (Tauris et al. 2017); for the fast-merging channel, the range is 0.5–1.5 hr. For each of DNS system we calculate v_{kick} and compare it to the maximum kick that a binary can withstand without being disrupted v_{max}

Table 3
The Relationship of "Radio Fraction" $f_{\rm radio}$ (Equation (A3)) and the "Gravitational-wave Fraction" $f_{\rm GW}$ (Equation (A4)) to k, the Coefficient Relating CO Core Mass and Supernova Kick (Equation (A2))

k (km s^{-1} $M_\odot^{-1}$)	$f_{\rm radio}$	$f_{\rm GW}$
100	0.084	0.083
200	0.084	0.083
300	0.082	0.083
400	0.059	0.083
500	0.042	0.083
600	0.02	0.081
700	0.004	0.06
800	0	0.034

Note. The radio fraction is stable for small values of k. However, when $k \gtrsim 400$ km s$^{-1} M_\odot^{-1}$, $f_{\rm radio}$ begins to drop appreciably, indicating that supernova kicks are efficiently disrupting slow-merging, massive DNS like GW190425 from the radio population. The gravitational-wave fraction is stable until $k \gtrsim 700$ km s$^{-1} M_\odot^{-1}$, at which point supernova kicks become so large that even tight, fast-merging binaries are disrupted, thereby depleting the GW190425–like DNS from the population observed with gravitational waves.

(Brandt & Podsiadlowski 1995). If $v_{\rm kick} > v_{\rm max}$, then the DNS is flagged as disrupted; otherwise, it remains intact.

We carry out the simulation for different values of k. For each value of k, we calculate the "radio fraction" $f_{\rm radio}$, defined as the fraction of surviving slow-merging DNS with $P_b > 1.5$ hr and total mass greater than the total mass of GW190425:

$$f_{\rm radio} = \frac{N(v_{\rm kick} < v_{\rm max} \,\&\, P_b > 1.5\ \text{hr} \,\&\, m_{\rm tot} > m_{\rm tot}^{\rm GW190425})}{N(v_{\rm kick} < v_{\rm max} \,\&\, P_b > 1.5\ \text{hr})}. \quad (A3)$$

The requirement that $P_b > 1.5$ hr is to take into account the fact that ultrarelativistic binaries are difficult to detect in radio (Pol et al. 2020). We expect $f_{\rm radio}$ to become smaller for sufficiently large values of k because slow-merging DNS are disrupted. Next, we calculate the "GW fraction" $f_{\rm GW}$, defined as the fraction of surviving fast-merging DNS with total mass greater than the total mass of GW190425:

$$f_{\rm GW} = \frac{N(v_{\rm kick} < v_{\rm max} \,\&\, m_{\rm tot} > m_{\rm tot}^{\rm GW190425})}{N(v_{\rm kick} < v_{\rm max})}. \quad (A4)$$

The results are summarized in Table 3. For values of $k \lesssim 300$ km s$^{-1} M_\odot^{-1}$, the fast-merging hypothesis has little explanatory power because the radio fraction is fairly stable at $f_{\rm radio} \approx 0.084$. Approximately 8% of the radio population are massive GW190425–like binaries, and these high-mass systems are not effectively disrupted by supernova kicks. However, when $k \gtrsim 400$ km s$^{-1} M_\odot^{-1}$, the radio fraction begins to fall appreciably, indicating that supernova are distorting the distribution of neutron star mass in radio-visible DNS. Thus— given our simple model—we find that $k \gtrsim 400$ km s$^{-1} M_\odot^{-1}$ is required in order for the fast-merging hypothesis to have explanatory power in accounting for the unusual mass of GW190425. In Figure 10, we show the kick velocity distribution for $k = 400$ km s$^{-1} M_\odot^{-1}$.[9] We find that a significant fraction of neutron star kicks are greater than 1000 km s^{-1},

---

[9] While a line with a slope of 400 km s$^{-1} M_\odot^{-1}$ can be drawn through the $v_{\rm kick}$– $m_{\rm core}$ relation in Mandel & Müller (2020), we require larger values of $v_{\rm kick}$ than allowed in that work in order for the fast-merging hypothesis to have explanatory power.
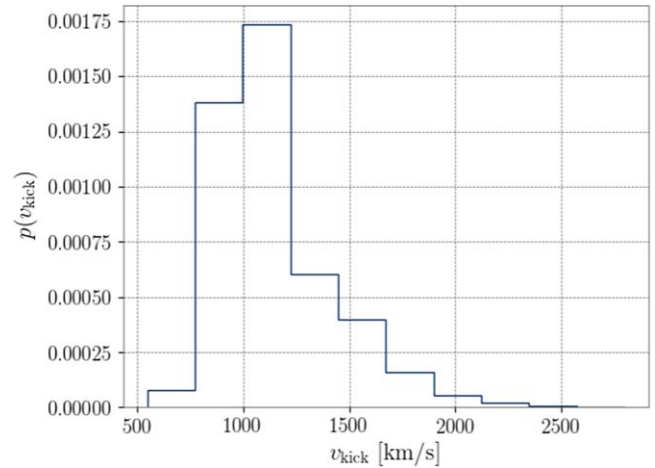

Figure 10. Histogram of the kick velocity for slow-merging DNS assuming $k = 400$ km s$^{-1} M_\odot^{-1}$ (see Equation (A2)). Given the assumptions of our model, this value of k produces sufficiently large kicks for the fast-merging hypothesis to efficiently deplete massive, GW190425–like binaries from the radio population. Large kick values $\gtrsim 1000$ km s^{-1} pose a challenge to conventional thinking about supernovae.

which is sometimes taken as the plausible maximum value. Some kicks in this model even exceed 2000 km s^{-1}. The exact shape of the supernova kick distribution required to support the fast-merging scenario is highly uncertain—a different parameterization could produce a substantially different result. However, it seems clear that large kicks ($\gg 1000$ km s^{-1}) are required for the fast-merging theory to have explanatory power.

Observations of pulsar proper motions indicate that neutron star kicks are typically a few hundred km s^{-1} (e.g., Hobbs et al. 2005), although some pulsars are observed to have velocities greater than 1000 km s^{-1} (Chatterjee et al. 2005; Hobbs et al. 2005; Tomsick et al. 2012). Hobbs et al. (2005) measure proper motions for PSRs B2011+38 and B2224+65, which imply both pulsars have velocities >1500 km s^{-1}. For PSR B2224 +65, this agrees with an independent velocity measurement based on the existence of a bow shock (the so-called "guitar nebula"; Cordes et al. 1993). PSR B1508 + 55 has a well-measured velocity of >1000 km s^{-1} based on VLBA measurements of its proper motion and parallax (Chatterjee et al. 2005).

A number of pulsars and central compact objects also have high inferred velocities (>1000 km s^{-1}) based on associations with supernova remnants (SNRs). PSR J1437-5959 has an inferred velocity >1000 km s^{-1} based on an association with the SNR G315.78−0.23 (Ng et al. 2012). SGR 0525−66 has a velocity of >1200 km s^{-1} based on association with SNR N49 (Rothschild et al. 1994), while the central compact object XMMU J172054.5−372652 in SNR G350.1−0.3 has an inferred velocity of 1400–2600 km s^{-1} (Lovchinsky et al. 2011). Similarly, RX J0822−4300 in the SNR Puppis A has a velocity of ~750–1500 km s^{-1} (Hui & Becker 2006). IGR J11014−6103, associated with the SNR MSH 1161A may be the fastest known pulsar with an inferred velocity of 2000–3000 km s^{-1} (Tomsick et al. 2012). Unfortunately, none of the neutron stars mentioned above have mass measurements (because typically mass measurements are only possible for neutron stars in binaries), so it is not possible to check if there is a correlation between large masses and high velocities.

For the fast-merging channel, $f_{\rm GW}$ is fairly stable until $k \gtrsim 700$ km s$^{-1} M_\odot$ at which point supernova kicks become so large that they begin to disrupt even tight, fast-merging

binaries. Interestingly, the entire range of k considered in Table 3 is consistent with the observed mass distributions of DNS in radio and gravitational waves. As noted above, small values of $k \lesssim 300\,\mathrm{km\,s^{-1}}M_\odot$ do not appreciably affect the shape of the radio distribution of DNS. However, because we find only mild statistical support for the fast-merging hypothesis, the radio data can be adequately explained by supposing that the radio DNS population contains massive GW190425 −like systems like the gravitational-wave population—we just have not seen one yet. This is not an unlikely possibility: given our model, the probability of not observing a radio DNS at least as massive as GW190425 from a set of 12 observations is 35%.

It is also possible that large kicks are not required to explain the absence of massive DNS in radio observations. Perhaps the simplest explanation is that the massive helium stars invoked in the fast-merging hypothesis do not reach the giant radii of less massive He stars (e.g., Laplace et al. 2020). If the maximum radius of these stars is only a few solar radii, then only binaries with $P_{\mathrm{orb}} \lesssim 12$ hr will interact. Therefore, the first neutron stars born in wide massive DNS may be unrecycled and thus more difficult to observe in radio (due to their short radio lifetimes). This hypothesis requires further investigation with detailed studies and may be tested observationally with LISA (Lau et al. 2020; Thrane et al. 2020).

ORCID iDs

Shanika Galaudage ⬡ https://orcid.org/0000-0002-1819-0215
Christian Adamcewicz ⬡ https://orcid.org/0000-0001-5525-6255
Xing-Jiang Zhu ⬡ https://orcid.org/0000-0001-7049-6468
Simon Stevenson ⬡ https://orcid.org/0000-0002-6100-537X
Eric Thrane ⬡ https://orcid.org/0000-0002-4418-3895

References

Aasi, J., Abbott, B. P., Abbott, R., et al. 2015, CQGra, 32, 074001
Abbott, B. P., Abbott, R., Abbott, T. D., et al. 2017, PhRvL, 119, 161101
Abbott, B. P., Abbott, R., Abbott, T. D., et al. 2019, ApJL, 882, L24
Abbott, B. P., Abbott, R., Abbott, T. D., et al. 2020, ApJL, 892, L3
Acernese, F., Agathos, M., Agatsuma, K., et al. 2015, CQGra, 32, 024001
Alsing, J., Silva, H. O., & Berti, E. 2018, MNRAS, 478, 1377
Andrews, J. J., Breivik, K., Pankow, C., D'Orazio, D. J., & Safarzadeh, M. 2020, ApJL, 892, L9
Andrews, J. J., & Mandel, I. 2019, ApJL, 880, L8
Andrews, J. J., & Zezas, A. 2019, MNRAS, 486, 3213
Armano, M., Audley, H., Auger, G., et al. 2016, PhRvL, 116, 231101
Ashton, G., Hübner, M., Lasky, P. D., et al. 2019, ApJS, 241, 27
Bae, Y.-B., Kim, C., & Lee, H. M. 2014, MNRAS, 440, 2714
Belczynski, K., Askar, A., Arca-Sedda, M., et al. 2018, A&A, 615, A91
Biscoveanu, S., Isi, M., Vitale, S., & Varma, V. 2020, arXiv:2007.09156
Brandt, N., & Podsiadlowski, P. 1995, MNRAS, 274, 461
Bransgrove, A., Levin, Y., & Beloborodov, A. 2018, MNRAS, 473, 2771
Breu, C., & Rezzolla, L. 2016, MNRAS, 459, 646
Cameron, A. D., Champion, D. J., Kramer, M., et al. 2018, MNRAS, 475, L57
Chatterjee, S., Vlemmings, W. H. T., Brisken, W. F., et al. 2005, ApJL, 630, L61
Chattopadhyay, D., Stevenson, S., Hurley, J. R., Rossi, L. J., & Flynn, C. 2020, MNRAS, 494, 1587
Chatziioannou, K., & Farr, W. M. 2020, PhRvD, 102, 064063
Clesse, S., & Garcia-Bellido, J. 2020, arXiv:2007.06481
Cordes, J. M., Romani, R. W., & Lundgren, S. C. 1993, Natur, 362, 133
Cromartie, H. T., Fonseca, E., Ransom, S. M., et al. 2020, NatAs, 4, 72
Dewi, J. D. M., & Pols, O. R. 2003, MNRAS, 344, 629
Ertl, T., Woosley, S. E., Sukhbold, T., & Janka, H. T. 2020, ApJ, 890, 51

Essick, R., & Landry, P. 2020, ApJ, 904, 80
Farrow, N., Zhu, X.-J., & Thrane, E. 2019, ApJ, 876, 18
Ferdman, R. D., Freire, P. C. C., Perera, B. B. P., et al. 2020, Natur, 583, 211
Ferdman, R. D., Stairs, I. H., Kramer, M., et al. 2014, MNRAS, 443, 2183
Fishbach, M., Essick, R., & Holz, D. E. 2020, ApJL, 899, L8
Foley, R. J., Coulter, D. A., Kilpatrick, C. D., et al. 2020, MNRAS, 494, 190
Fong, W., & Berger, E. 2013, ApJ, 776, 18
Fonseca, E., Stairs, I. H., & Thorsett, S. E. 2014, ApJ, 787, 82
Fryer, C. L., Belczynski, K., Wiktorowicz, G., et al. 2012, ApJ, 749, 91
Grindlay, J., Portegies Zwart, S., & McMillan, S. 2006, NatPh, 2, 116
Gupta, A., Gerosa, D., Arun, K. G., et al. 2020, PhRvD, 101, 103036
Haniewicz, H. T., Ferdman, R. D., Freire, P. C. C., et al. 2021, MNRAS, 500, 4620
Hobbs, G., Lorimer, D. R., Lyne, A. G., & Kramer, M. 2005, MNRAS, 360, 974
Hui, C. Y., & Becker, W. 2006, A&A, 457, L33
Ivanova, N., Belczynski, K., Kalogera, V., Rasio, F. A., & Taam, R. E. 2003, ApJ, 592, 475
Jacoby, B. A., Cameron, P. B., Jenet, F. A., et al. 2006, ApJL, 644, L113
Ji, A. P., Frebel, A., Chiti, A., & Simon, J. D. 2016, Natur, 531, 610
Kiziltan, B., Kottas, A., De Yoreo, M., & Thorsett, S. E. 2013, ApJ, 778, 66
Kobayashi, C., Karakas, A. I., & Lugaro, M. 2020, ApJ, 900, 179
Korol, V., & Safarzadeh, M. 2021, MNRAS, in press (doi:10.1093/mnras/stab310)
Kramer, M., Stairs, I. H., Manchester, R. N., et al. 2006, Sci, 314, 97
Kruckow, M. U. 2020, A&A, 639, A123
Kyutoku, K., Fujibayashi, S., Hayashi, K., et al. 2020, ApJL, 890, L4
Landry, P., Essick, R., & Chatziioannou, K. 2020, PhRvD, 101, 123007
Laplace, E., Götberg, Y., de Mink, S. E., Justham, S., & Farmer, R. 2020, A&A, 637, A6
Lau, M. Y. M., Mandel, I., Vigna-Gómez, A., et al. 2020, MNRAS, 492, 3061
Lovchinsky, I., Slane, P., Gaensler, B. M., et al. 2011, ApJ, 731, 70
Lynch, R. S., Freire, P. C. C., Ransom, S. M., & Jacoby, B. A. 2012, ApJ, 745, 109
Lynch, R. S., Swiggum, J. K., Kondratiev, V. I., et al. 2018, ApJ, 859, 93
MacLeod, M., & Ramirez-Ruiz, E. 2014, ApJL, 798, L19
Madau, P., & Dickinson, M. 2014, ARA&A, 52, 415
Mandel, I., & Müller, B. 2020, MNRAS, 499, 3214
Mandel, I., Müller, B., Riley, J., et al. 2021, MNRAS, 500, 1380
Martinez, J. G., Stovall, K., Freire, P. C. C., et al. 2015, ApJ, 812, 143
Müller, B., Heger, A., Liptai, D., & Cameron, J. B. 2016, MNRAS, 460, 742
Neijssel, C. J., Vigna-Gómez, A., Stevenson, S., et al. 2019, MNRAS, 490, 3740
Ng, C. Y., Bucciantini, N., Gaensler, B. M., et al. 2012, ApJ, 746, 105
O'Shaughnessy, R., & Kim, C. 2010, ApJ, 715, 230
Papenfort, L. J., Gold, R., & Rezzolla, L. 2018, PhRvD, 98, 104028
Pol, N., McLaughlin, M., Lorimer, D. R., & Garver-Daniels, N. 2020, arXiv:2008.03842
Radice, D., Perego, A., Hotokezaka, K., et al. 2018, ApJ, 869, 130
Romero-Shaw, I. M., Farrow, N., Stevenson, S., Thrane, E., & Zhu, X.-J. 2020, MNRAS, 496, L64
Rothschild, R. E., Kulkarni, S. R., & Lingenfelter, R. E. 1994, Natur, 368, 432
Safarzadeh, M., Ramirez-Ruiz, E., Andrews, J. J., et al. 2019, ApJ, 872, 105
Safarzadeh, M., Ramirez-Ruiz, E., & Berger, E. 2020, ApJ, 900, 13
Snaith, O., Haywood, M., Di Matteo, P., et al. 2015, A&A, 578, A87
Speagle, J. S. 2020, MNRAS, 493, 3132
Spera, M., Mapelli, M., & Bressan, A. 2015, MNRAS, 451, 4086
Talbot, C., & Thrane, E. 2018, ApJ, 856, 173
Tauris, T. M., Kramer, M., Freire, P. C. C., et al. 2017, ApJ, 846, 170
Thrane, E., Osłowski, S., & Lasky, P. D. 2020, MNRAS, 493, 5408
Thrane, E., & Talbot, C. 2019, PASA, 36, E010
Tomsick, J. A., Bodaghee, A., Rodriguez, J., et al. 2012, ApJL, 750, L39
van Leeuwen, J., Kasian, L., Stairs, I. H., et al. 2015, ApJ, 798, 118
Vigna-Gómez, A., Neijssel, C. J., Stevenson, S., et al. 2018, MNRAS, 481, 4009
Vitale, S., Gerosa, D., Farr, W. M., & Taylor, S. R. 2020, arXiv:2007.05579
Weisberg, J. M., Nice, D. J., & Taylor, J. H. 2010, ApJ, 722, 1030
Ye, C. S., Fong, W.-f., Kremer, K., et al. 2020, ApJL, 888, L10
Zevin, M., Kremer, K., Siegel, D., et al. 2019, ApJ, 886, 4
Zhu, X.-J., & Ashton, G. 2020, ApJL, 902, L12
Zhu, X.-J., Thrane, E., Osłowski, S., Levin, Y., & Lasky, P. D. 2018, PhRvD, 98, 043002